Journal of *Marine Science and Engineering*

MDPI

Article

Fluid Flow Simulation for Predicting Bottomhole Pressure That Considers Wellbore Storage Effects Under Shut-In Conditions in Deepwater Drilling

Yanli Guo [1,*], Yonghai Gao [2], Qingtao Gong [1], Lifen Hu [1], Yongyi Jiang [1] and Baojiang Sun [2,*]

[1] Ulsan Ship and Ocean College, Ludong University, Yantai 264025, China; gongqt@ldu.edu.cn (Q.G.); hulifen@ldu.edu.cn (L.H.); jyyldu@ldu.edu.cn (Y.J.)
[2] School of Petroleum Engineering, China University of Petroleum (East China), Qingdao 266580, China; upcgaoyh@126.com
* Correspondence: guoyanli@ldu.edu.cn (Y.G.); sunbj@upc.edu.cn (B.S.)

Abstract: Under shut-in conditions in deepwater drilling, the gas invading the bottomhole ascends along the wellbore and accumulates at the wellhead, forming a high-pressure trap, challenging wellbore pressure prediction and control. The accurate prediction of bottomhole pressure is essential for well control during shut-in conditions. In this study, a new bottomhole pressure prediction model that considers wellbore storage effects was developed to address gas invasion issues during shut-in conditions in deepwater drilling. This model incorporates factors such as the wellbore elasticity, fluid compressibility, and drilling fluid filtration loss. The calculated values show good agreement with experimental values, with the average absolute and relative errors of 2.095 $\times$ 10^{-2} MPa and 3.71%, respectively. Meanwhile, the results indicate that the bottomhole pressure initially increases logarithmically over time and then transitions to a linear increase, and the residual flow and gas ascent significantly influence the bottomhole pressure. Finally, the effects of various parameters on the bottomhole pressure were evaluated. Larger initial pressure differential, exposed thickness, and formation permeability accelerate the increase in bottomhole pressure during residual flow stage, while smaller filter cake permeability and drilling fluid viscosity quicken its increase during gas ascent stage. Drilling fluid density affects the initial pressure and the residual flow duration. The findings of this study would provide theoretical support for well control operations in deepwater drilling.

Keywords: bottomhole pressure; wellbore storage effect; shut-in; sensitivity analysis; deepwater drilling

check for updates

Academic Editor: Atilla Incecik

Received: 2 December 2024
Revised: 22 December 2024
Accepted: 26 December 2024
Published: 27 December 2024

Citation: Guo, Y.; Gao, Y.; Gong, Q.; Hu, L.; Jiang, Y.; Sun, B. Fluid Flow Simulation for Predicting Bottomhole Pressure That Considers Wellbore Storage Effects Under Shut-In Conditions in Deepwater Drilling. *J. Mar. Sci. Eng.* **2025**, *13*, 22. https://doi.org/10.3390/jmse13010022

Copyright: © 2024 by the authors. Licensee MDPI, Basel, Switzerland. This article is an open access article distributed under the terms and conditions of the Creative Commons Attribution (CC BY) license (https://creativecommons.org/licenses/by/4.0/).

1. Introduction

Drilling is the most effective and direct method for oil and gas exploration and development, which has increasingly shifted its focus to deepwater areas in recent years [1,2]. Deepwater drilling technology has advanced significantly since 1965, evolving from an initial operating water depth of 183 m to its current capability of operating at depths of up to 3600 m and beyond [3,4]. However, the complex marine and geological environments often cause gas invasion, posing one of the main challenges, which could lead to blowouts, financial losses and damages to the drilling crew [5]. During deepwater drilling, scenarios such as shallow gas, natural gas reservoirs, and hydrate reservoirs can lead to gas invasion [6–8]. Following gas invasion, the flow pattern within the wellbore becomes complex, transitioning from single-phase flow to gas–liquid two-phase flow [9]. Specifically,

in deepwater drilling, under shut-in conditions, the gas invading the bottomhole ascends along the wellbore and accumulates at the wellhead, forming a high-pressure trap. When the trapped gas undergoes hydrate phase transitions, gas consumption occurs, causing dynamic variations in the wellhead backpressure, which pose a significant challenge in wellbore pressure control [10,11]. Therefore, accurately predicting the bottomhole pressure is critical for well control operations under shut-in conditions in deepwater drilling.

The wellbore fluid flow model for deepwater drilling provides a theoretical basis for accurate prediction and control of the wellbore pressure. Scholars worldwide have developed wellbore flow models for single-phase and multiphase flow conditions tailored to various operational conditions. In deepwater drilling, the impact of a phase transition of natural gas hydrates on the multiphase flow pattern in the wellbore cannot be ignored. Researchers such as Sun et al. [12] and Wang et al. [13] have incorporated hydrate phase effects into existing multiphase flow models and have developed a seven-component multiphase flow computation method for wellbore flow, which has been applied in several oilfields in China. Ren et al. [14] addressed the significant discrepancies between calculated and actual wellbore pressures under blowout shut-in conditions by establishing a wellbore pressure calculation model based on seepage theory, well testing theory, and multiphase flow theory. Wan et al. [15] developed an annular multiphase flow calculation model that considers the properties of acidic gases after they invade the wellbore. He et al. [16] integrated managed pressure drilling (MPD) technology, advanced the multiphase flow control model for MPD, and revealed the sensitivities of the bottomhole pressure and temperature to various parameters under two control methods: constant bottomhole pressure and constant wellhead pressure. They also compared the effects of acidic gas invasion and neutral gas invasion on wellbore pressure control. For deepwater dual-gradient drilling, researchers such as Halkyard et al. [17], Marbun et al. [18], and Li et al. [19] developed temperature and pressure calculation models suitable for various dual-gradient drilling methods, including subsea lifting pumps, hollow ball injection, and controlled mud level (CML) operations. Focusing on the characteristics of deep marine oil and gas reservoirs, Xu [20] developed a numerical algorithm for transient multiphase flow in the wellbore and analyzed the dynamic response characteristics of various flow parameters within the wellbore. Additionally, some scholars have used commercial software to simulate fluid flow in wellbores. For example, Rashid et al. [21] conducted simulations of hot fluid flow in a wellbore using ANSYS Fluent Version 16, revealing the relationship between turbulence, heat transfer, and production efficiency. That is, since Leblanc et al. [22] introduced the first mathematical model for gas kick control, research on the modeling of multiphase flow in wellbores has transitioned from steady-state to transient models, from isothermal to non-isothermal models, and from models without phase changes to models that account for phase changes [10].

Building on traditional two-phase gas–liquid flow, some models have incorporated hydrate and supercritical phases, while others have accounted for scenarios such as blowout shut-in, dual-gradient drilling, and MPD. These models have been successfully applied under specific conditions. However, significant differences persist between calculated and actual bottomhole pressures during shut-in operations in deepwater drilling, particularly when the minor gas invasion occurs during extended shut-in periods, such as those for typhoon avoidance. The existing models cannot accurately describe the characteristics of changes in bottomhole pressure under shut-in conditions in deepwater drilling. Thus, this indicates that further improvements to the model are necessary to enable accurate prediction of bottomhole pressure. In this study, considering the storage effects of the wellbore during shut-in operations, factors such as wellbore elasticity, fluid compressibility, and drilling fluid loss were incorporated to establish a new model for predicting bottomhole

pressure under shut-in conditions in deepwater drilling. The validity and accuracy of the model were verified, and the influences of the reservoir and drilling parameters on the bottomhole pressure were elucidated.

2. Model

2.1. Concepts and Principles

During the shut-in period following gas invasion caused by a negative pressure differential, the two-phase gas–liquid flow process in the wellbore can be divided into three stages: the residual flow stage, the gas ascent stage, and the drilling fluid filtration loss stage. Changes in the wellbore pressure are the result of the combined effects of the residual flow, gas ascent, and drilling fluid filtration loss. Figure 1 illustrates the fluid flow in the wellbore after gas invasion under shut-in conditions during deepwater drilling.

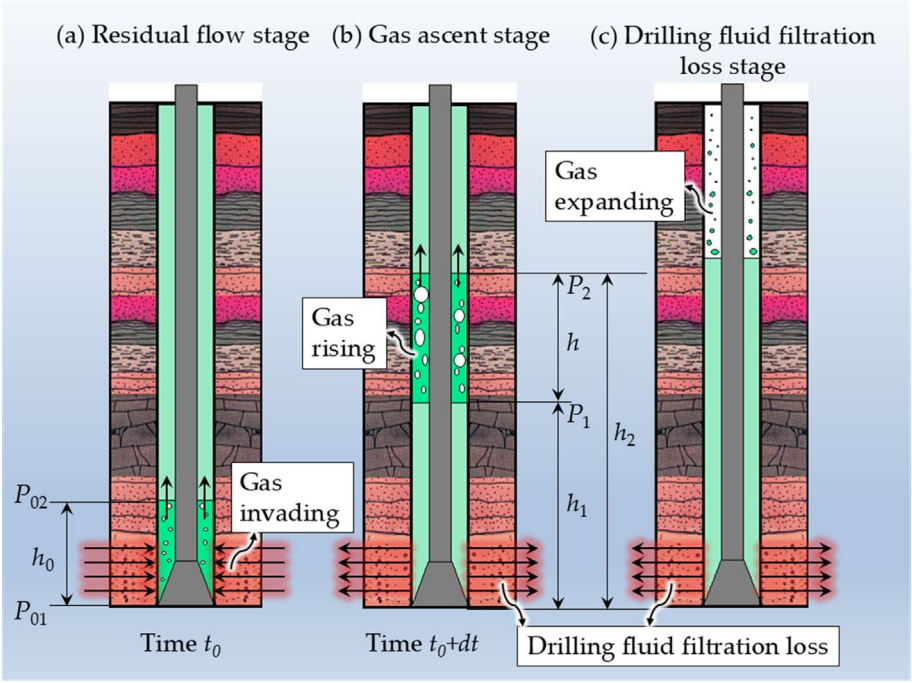


Figure 1. Schematic diagram of fluid flow in the wellbore after gas invasion under shut-in conditions in deepwater drilling.

(1) Residual flow stage

During this stage, the formation pressure is greater than the bottomhole pressure. In the initial stage of a shut-in period due to gas invasion, formation gases continue to invade the wellbore as a result of the pressure differential. In the semi-enclosed space of the wellbore, the invading gases compress the wellbore fluids and expand the wellbore volume, leading to an increase in the wellbore pressure. When the bottomhole pressure approaches the formation pressure, no further gases will invade the wellbore as the pressure differential decreases.

(2) Gas ascent stage

At the beginning of this stage, the bottomhole pressure is equal to formation pressure. The gases already present in the wellbore continue to ascend from the bottomhole to the wellhead due to the density differential. As the gases rise, they experience a continuous decrease in pressure, leading to their expansion and causing a further increase in bottomhole pressure. When the bottomhole pressure exceeds the formation pressure, the drilling

fluid in the open-hole section of the wellbore begins to undergo filtration loss under the pressure differential.

(3) Drilling fluid filtration loss stage

During this stage, the gas reaches the wellhead, and the wellbore pressure reaches a maximum value. At the initial moment, the bottomhole pressure is higher than the formation pressure, causing the drilling fluid to continue to undergo filtration loss, which leads to a decrease in the wellbore pressure. As the bottomhole pressure approaches the formation pressure, the fluid loss ceases and the wellbore pressure stabilizes.

In summary, in the residual flow stage, gas ascent also occurs, but the residual flow is the main factor controlling the wellbore pressure changes. In the gas ascent stage, the wellbore pressure changes are driven by the combined effect of the gas ascent and drilling fluid filtration loss. In the drilling fluid filtration loss stage, the drilling fluid loss controls the changes in the wellbore pressure.

2.2. Model Development

2.2.1. Residual Flow Stage

Considering the elasticity of the wellbore and the compressibility of the fluid, according to the law of mass conservation, after shut-in, the volume of the formation gas that invades the wellbore is equivalent to the sum of the decreases in the volumes of the pre-existing gas and drilling fluid in the wellbore due to compression, as well as the increased volume of the wellbore due to expansion. This relationship can be expressed as follows:

$$V_{in} = V_g C_g dP_w + V_l C_l dP_w + V_c C_c dP_w, \tag{1}$$

where V_{in}, V_g, V_l, and V_c are the volume of the formation gas invading the wellbore, the volume of the pre-existing gas in the wellbore, the volume of the pre-existing drilling fluid in the wellbore, and the volume of the wellbore (m^3), respectively, C_g, C_l, and C_c, are the compressibility coefficients of the gas, drilling fluid, and wellbore (Pa^{-1}), respectively. The compression coefficient of water-based drilling fluid decreases continuously with increasing pressure and exhibits a decrease followed by an increase with rising temperature, generally ranging from 3.7 to 5×10^{-4} MPa^{-1} [23]. In comparison, the compressibility coefficient of the wellbore is much smaller than that of the drilling fluid and gas. To simplify calculations, the compressibility coefficient of the drilling fluid is set to 4.5×10^{-4} MPa^{-1}, and that of the wellbore is set to 0.05×10^{-4} MPa^{-1} [14].

(1) The volume of gas in the wellbore: The volume of formation gas that invades the wellbore from time t_0 to $t_0 + dt$ is expressed as follows:

$$V_{in} = Q_g(t_0)dt. \tag{2}$$

The accumulated volume of formation gas that invades the wellbore during time period $[0, t_0]$, under the wellbore pressure conditions at time t_0, is expressed as follows:

$$V_{acc} = \int_0^{t_0} Q_g(t)dt. \tag{3}$$

Thus, under the wellbore pressure conditions, the total gas volume in the wellbore at time t_0 is

$$V_g = V_{in} + V_{acc} = Q_g(t_0)dt + \int_0^{t_0} Q_g(t)dt. \tag{4}$$

(2) The volume of the drilling fluid in the wellbore at time t_0 is

$$V_l = V_c - V_{acc} = V_c - \int_0^{t_0} Q_g(t)dt. \quad (5)$$

(3) The wellbore volume can be determined based on the structure of the well depth and the dimensions of the drill string.

Substituting Equations (2)–(5) into Equation (1) yields

$$Q_g(t_0)dt = \left[\left(\int_0^{t_0} Q_g(t)dt\right) + Q_g(t_0)dt\right]C_g dP_w + \left[V_c - \int_0^{t_0} Q_g(t)dt\right]C_l dP_w + V_c C_c dP_w. \quad (6)$$

where V_{acc} is the accumulated volume of formation gas that invades the wellbore (m^3), and Q_g is the gas volumetric flow rate (m^3/s).

According to fluid hydrostatics, the pressures at the trailing edge, leading edge, and wellhead of the gas are as follows:

$$\begin{cases} P_{01} = P_w \\ P_{02} = P_w - \left[\rho_g E_g + (1 - E_g)\rho_l\right]gh_0 \\ P_C = P_{02} - \rho_l g(H - h_0) \end{cases}, \quad (7)$$

where P_{01}, P_{02}, and P_C are the pressures at the trailing and leading edges of the gas and at the wellhead (Pa), respectively, E_g is the average gas fraction in the cross-section of the gas–liquid mixture segment, H is the well depth (m), h_0 is the height of the gas–liquid mixture segment (m), and ρ_g and ρ_l are the average densities of the gas and drilling fluid (kg/m^3), respectively.

2.2.2. Gas Ascent Stage

Based on the parameters obtained at the end of the residual flow stage, the initial gas invasion height, gas invasion volume, and wellbore pressure distribution can be determined for the gas ascent stage, which provide the initial conditions for this stage. Referring to Figure 1, the gas ascent process is then analyzed.

Considering the elasticity of the wellbore and the compressibility of the fluids (including both the drilling fluid and the gas invading the wellbore) and in accordance with the law of mass conservation, the increased gas volume due to expansion is equal to the sum of the decreased volume of drilling fluid due to compression, the decreased volume of the drilling fluid due to loss to the formation, and the increased wellbore volume due to expansion:

$$\Delta V_g = \Delta V_f + V_l C_l dP_w + V_c C_c dP_w, \quad (8)$$

where ΔV_g and ΔV_f are the volume changes caused by gas expansion and the volume of the drilling fluid lost to the formation (m^3), respectively.

(1) Increased gas volume due to gas expansion

Due to pressure differences along the wellbore, the density and size of the bubbles vary, which results in the gas bubbles at the leading edge of the gas–liquid mixture segment having a different ascent velocity compared to those at the trailing edge. The ascent heights of the bubbles at the leading and trailing edges from time t_0 to $t_0 + dt$, as well as the height of the gas–liquid mixture segment, are as follows:

$$\begin{cases} h_1 = v_1 dt \\ h_2 = v_2 dt + h_0 \\ h = h_2 - h_1 \end{cases}, \quad (9)$$

where h_1, h_2, and h are the heights of the trailing edge and leading edge of the gas and the gas–liquid mixture segment (m), respectively, and v_1 and v_2 are the ascent velocities of the trailing edge and leading edge of the gas (m/s), respectively.

The wellhead pressure and the pressures at the top and bottom of the gas–liquid mixture segment can be determined based on the ascent position of the gas–liquid mixture segment:

$$\begin{cases} P_1 = P_w - \rho_l g h_1 \\ P_2 = P_1 - \left[\rho_g E_g + (1 - E_g)\rho_l\right] g h \\ P_C = P_2 - \rho_l g (H - h_2) \end{cases}, \quad (10)$$

where P_1, P_2, and P_C are the pressures at the trailing edge and leading edge of the gas and at the wellhead (Pa), respectively, E_g is the average gas fraction in the cross-section of the gas–liquid mixture segment, H is the well depth (m), and ρ_g and ρ_l are the average densities of the gas and drilling fluid (kg/m^3), respectively.

Using the gas state equation, the average density and volume of the gas in the gas–liquid mixture segment can be calculated. The difference in the gas volume between times $t_0 + dt$ and t_0 represents the increased gas volume due to gas expansion.

(2) Volume of drilling fluid lost to the formation

Given the bottomhole pressure differential and the physical properties of the drilling fluid and filter cake, the volume of the drilling fluid lost to the formation can be calculated using the static fluid filtration loss equation [23]:

$$\Delta V_f = S\sqrt{\frac{K_f}{\mu_m}\left(\frac{f_{sc}}{f_{sm}} - 1\right)(P_w - P_e)t}, \quad (11)$$

where f_{sm} is the solid content in the drilling fluid (%), f_{sc} is the solid content in the filter cake (%), K_f is the permeability of the filter cake (10^{-3} μm^2), S is the open-hole cross sectional area of the wellbore (m^2), μ_m is the viscosity of the drilling fluid (mPa·s), P_w is the bottomhole pressure (Pa), P_e is the formation pressure (Pa), and t is the filtration loss time (min).

2.2.3. Drilling Fluid Filtration Loss Stage

In the drilling fluid filtration loss stage, the gas has fully reached the wellhead. The drilling fluid loss causes the wellbore pressure to begin to decrease. This decrease in pressure results in the expansion of the wellbore fluids and the contraction of the wellbore. In this stage, the volume of the drilling fluid lost to the formation is equal to the sum of the increases in the volume of gas and drilling liquid due to expansion and the decreased volume of wellbore due to contraction. It can be expressed as follows:

$$\Delta V_f = \Delta V_g + V_l C_l dP_w + V_c C_c dP_w. \quad (12)$$

The methods for determining each parameter in this equation are the same as those described above.

2.2.4. Determination of Allowable Wellbore Pressure

After gas invasion, as the gas ascends within the wellbore, the wellbore pressure increases, which may compromise the integrity of the wellbore by exceeding the casing's internal pressure resistance or the formation fracturing pressure. Therefore, control measures such as well-killing operations must be implemented before this occurs. The allowable wellbore pressure is determined as follows: the wellbore pressure at the casing shoe or the weakest point in the open-hole formation must not exceed the smaller of the forma-

tion fracture pressure and the casing's internal pressure resistance strength. Additionally, the wellhead pressure must not exceed the pressure-bearing capacity of the wellhead equipment. This is expressed as follows:

$$\begin{cases} P_f < \min\left\{P_{fshoe}, P_{fweak}, P_{ri}\right\} \\ P_C < P_{C\max} \end{cases}, \tag{13}$$

where P_f is the wellbore pressure at the casing shoe or the weakest point in the open-hole formation (Pa), P_{fshoe} is the formation fracturing pressure at the casing shoe (Pa), P_{fweak} is the formation fracturing/leak-off pressure at the weakest point in the open-hole formation (Pa), P_{ri} the casing's internal pressure resistance strength (Pa), P_C is the wellhead backpressure (Pa), and P_{Cmax} is the pressure-bearing capacity of the wellhead equipment (Pa).

2.3. Auxiliary Equations

Auxiliary equations are used to calculate the gas density, gas viscosity, gas invasion volume, initial bubble diameter, and gas ascent velocity.

Specifically, based on extensive previous research, the gas density is calculated using the gas state equation, and the gas compression factor is determined using the DPR empirical formula [24]. The gas viscosity is calculated using the semi-empirical Lee–Gonzalez–Eakin method [25]. Based on the mathematical model of seepage, the following velocity of gas invasion into the wellbore is obtained [26].

$$dQ = \frac{\pi T_a Z_a}{P_a T \overline{\mu} \overline{Z}} K_P \cdot \left(P_e^2 - P_w^2(x)\right) dx, \tag{14}$$

where Q is the gas volumetric flow rate (m^3/s), P_a is the pressure under standard condition (Pa), T_a and T are the temperatures under standard and formation conditions (K), respectively, Z_a and Z are the gas compressibility factors under standard and formation conditions, respectively, μ is the gas viscosity (mPa·s), K_P is the overall seepage coefficient.

The initial bubble diameter is determined based on the formation porosity, pore size, and gas invasion volume, and herein, the Anagbo–Brimacombe–Wraith model is used [27].

$$D_{eq} = 0.87\left(\frac{\rho_g}{\rho_l}\right)^{-0.25}\left(\frac{D_0}{2g}\right)^{0.5} Q_g, \tag{15}$$

where D_{eq} is the equivalent diameter of bubbles (mm), D_0 is the diameter of the nozzle (mm), ρ_l is the liquid density (kg/m^3), ρ_g is the gas density (kg/m^3), Q_g is the gas flow rate (m^3/s).

The gas ascent velocity depends on the flow patterns of gas–liquid two-phase flow in the wellbore [13]. The gas ascent velocity under bubble flow is calculated using the following formula:

$$v_g = 1.53\left[\frac{g(\rho_l - \rho_g)\sigma}{\rho_l^2}\right]^{0.25}, \tag{16}$$

while the gas ascent velocity under slug flow is calculated using the following formula:

$$v_g = 0.35\left[\frac{gd(\rho_l - \rho_g)}{\rho_l}\right]^{0.5}. \tag{17}$$

Herein, the flow patterns of gas–liquid two-phase flow in the wellbore is generally considered to transition from bubble flow to slug flow when the void fraction exceeds

0.07 [28]. Thus, the average value of the void fraction in section $h(x)$ can be expressed as follows:

$$E_g = \frac{M_g}{\rho_g(Ah(x))}. \tag{18}$$

where σ is the gas–liquid interfacial tension (mN/m), d is the inner diameter of wellbore (m), and M_g is the gas quality invading the wellbore (kg).

2.4. Solution Methodology

The solution methodology involves step-by-step calculations based on time increments. The steps of the methodology are presented below (as shown in Figure 2).

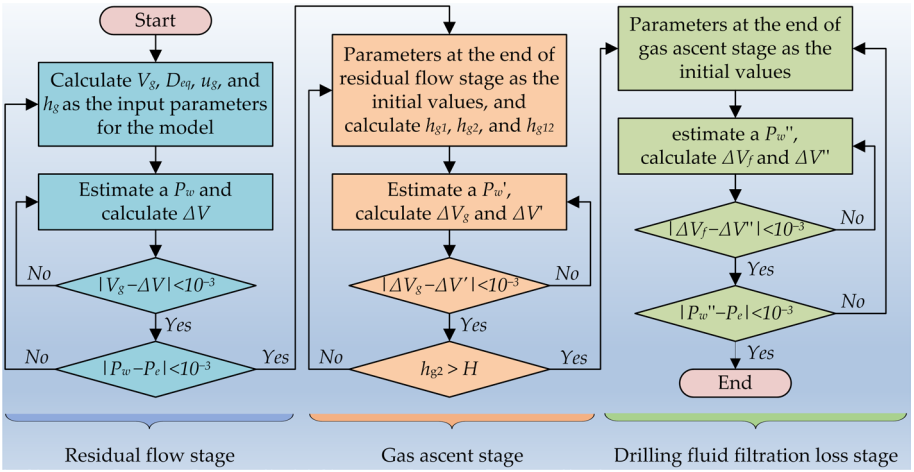


Figure 2. Solution flowchart.

Step 1. Calculate the gas invasion volume (V_g) within a unit time step, determine the equivalent diameter of the bubble (D_{eq}), and calculate the bubble ascent velocity (u_g), thereby determining the gas ascent height (h_g) within the unit time step.

Step 2. Estimate the change in the bottomhole pressure (P_w), and based on this, calculate the decreased volume of gas in the wellbore due to gas compression, the decreased volume of the liquid in the wellbore due to liquid compression, and the increased volume of the wellbore due to wellbore expansion. The sum of these three is denoted as ΔV.

Step 3. If $|V_g - \Delta V| < 10^{-3}$, then proceed to the next step; otherwise, re-estimate P_w and return to step 2.

Step 4. If $|P_w - P_e| < 10^{-3}$, then proceed to the next step; otherwise, calculate for the next time step and return to step 1.

Step 5. Use the parameters at the end of the residual flow stage as the initial values for the gas ascent stage, and calculate the trailing-edge height (h_{g1}), leading-edge height (h_{g2}), and length of the gas–liquid mixture segment (h_{g12}) within the unit time step.

Step 6. Estimate the change in the bottomhole pressure (P'_w), and under this condition, calculate the increased volume due to the gas expansion (ΔV_g), the increased volume due to drilling fluid compression, the volume of the drilling fluid lost to the formation, and the increased volume due to wellbore expansion. The sum of the latter three is denoted as $\Delta V'$.

Step 7. If $|\Delta V_g - \Delta V'| < 10^{-3}$, then proceed to the next step; otherwise, re-estimate P'_w and return to step 6.

Step 8. If $h_{g2} > H$ (wellbore depth), then proceed to the next step; otherwise, calculate for the next time step and return to step 5.

Step 9. Use the parameters at the end of the gas ascent stage as the initial values for the drilling fluid filtration loss stage, and estimate the change in the bottomhole pressure (P''_w) within a unit time step.

Step 10. Calculate the drilling fluid loss (ΔV_f) under the current conditions, as well as the increased gas volume due to gas expansion at the wellhead, the increased volume of the drilling fluid due to its expansion, and the increased volume due to wellbore contraction. The sum of the latter three is denoted as $\Delta V''$.

Step 11. If $\left|\Delta V_f - \Delta V''\right| < 10^{-3}$, then proceed to the next step; otherwise, re-estimate P_w'' and return to step 10.

Step 12. If $|P_w - P_e| < 10^{-3}$, then the calculation is complete; otherwise, calculate for the next time step and return to step 10.

2.5. Model Validation

The experimental values from an experiment on the variation of bottomhole pressure under simulated shut-in conditions are used to validate the model's effectiveness and accuracy [29]. Figure 3 shows the comparison between calculated values and experimental values. It can be seen that the calculated values of this model are in good agreement with the experimental values. The average absolute error between them is 2.095×10^{-2} MPa, with a relative error 3.71%, and the maximum absolute error is 5.213×10^{-2} MPa, with a maximum relative error of 19.56%. Additionally, these calculated and experimental values in Figure 3 also reflect the three stages of fluid flow in the wellbore after gas invasion under shut-in conditions. Under the simulated operating conditions of this experiment, it can be observed: (1) In the residual flow stage (before point A), the bottom pressure increases logarithmically, with an initially fast increase in pressure over a relatively short duration. (2) When the bottom pressure reaches the injection pressure, it transitions to the gas ascent stage (between point A and point B). Due to the gas rising under pressure, the bottom pressure increases linearly. As the gas approaches the top, the bottom pressure reaches its maximum, and this process is relatively long-lasting. (3) In the fluid filtration loss stage (after point B), due to the continuous fluid loss, the bottom pressure decreases logarithmically. As the bottom pressure approaches the injection pressure, it ceases to change. In summary, this model can be used to study the variations in the bottomhole pressure under gas invasion during a shut-in period in deepwater drilling.

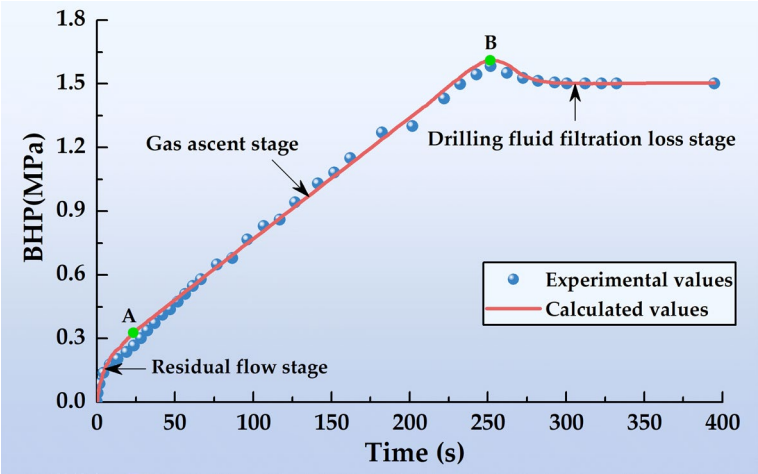


Figure 3. Comparison between calculated and experimental values. The BHP represents bottomhole pressure.

3. Results and Discussion

A case study was conducted to analyze the variations in the bottomhole pressure under negative pressure differential-induced gas invasion during a shut-in period. The basic parameters for the case study are presented in Table 1.

Table 1. Basic parameters of the case study.

Parameter	Value	Parameter	Value
water depth (m)	1000	drilling fluid density (kg/m^3)	1400
well depth (m)	3000	drilling fluid viscosity (mPa·s)	20
wellbore radius (m)	0.108	drilling fluid solid content	0.05
wellhead temperature (°C)	40	filter cake solid content	0.15
exposed reservoir thickness (m)	1	filter cake permeability (μm^2)	1×10^{-8}
formation pressure (MPa)	50	formation permeability (μm^2)	10×10^{-3}
formation temperature (°C)	85	methane critical temperature (°C)	−82.6
supply radius (m)	500	methane critical pressure (MPa)	4.59

3.1. Effect of Formation Pressure on Bottomhole Pressure

The simulation was conducted using an initial bottomhole pressure of 41.16 MPa and various formation pressures of 45 MPa, 50 MPa, and 55 MPa (corresponding bottomhole pressure differentials are 3.84 MPa, 8.84 MPa, and 13.84 MPa, respectively). The other parameters were held constant. The simulated bottomhole pressure variations over time under different formation pressures are shown in Figure 4. Taking the 50 MPa formation pressure curve as an example, the bottomhole pressure increases from 41.16 MPa to 50 MPa, exhibiting a logarithmic trend. That is, it shows an initially rapid rate of increase that slows down over time. This stage, characterized by a relatively short duration with a rapid pressure increase, corresponds to the residual flow stage. When the bottomhole pressure reaches the formation pressure, the process transitions to the gas ascent stage, during which the bottomhole pressure increases linearly due to the pressurized ascent of the gas. Once the bottomhole pressure becomes equal to the formation pressure, no additional gas invades the wellbore. At this stage, the rates of increase in the bottomhole pressure under different formation pressures are nearly identical. Figure 4 also shows that greater initial pressure differentials at the bottomhole resulting in faster pressure increases and longer residual flow stage durations.

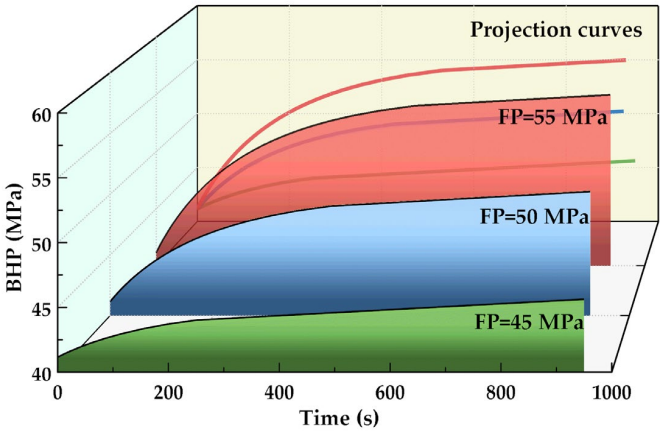


Figure 4. Variations in bottomhole pressure over time under different formation pressures. The BHP represents bottomhole pressure, and the FP represents formation pressure.

3.2. Effect of Exposed Reservoir Thickness on Bottomhole Pressure

The simulation was conducted using an initial bottomhole pressure of 41.16 MPa, a fixed formation pressure of 50 MPa, and exposed reservoir thicknesses of 1 m, 3 m, and 5 m. The other parameters were the same in Section 3.1. The simulated bottomhole pressure variations over time under different exposed reservoir thicknesses are shown in Figure 5. It can be seen that the bottomhole pressure shows similar trends for different exposed reservoir thicknesses; that is, it initially exhibits a logarithmic increase before transitioning to a linear increase over time. The exposed reservoir thickness significantly influences the variations in the bottomhole pressure during the residual flow stage. The

larger the exposed reservoir thickness, the more quickly the bottomhole pressure reaches the formation pressure. During the residual flow stage, a larger exposed reservoir thickness allows more gas to invade the wellbore per unit time, and consequently, it takes less time for the bottomhole pressure to reach the formation pressure.

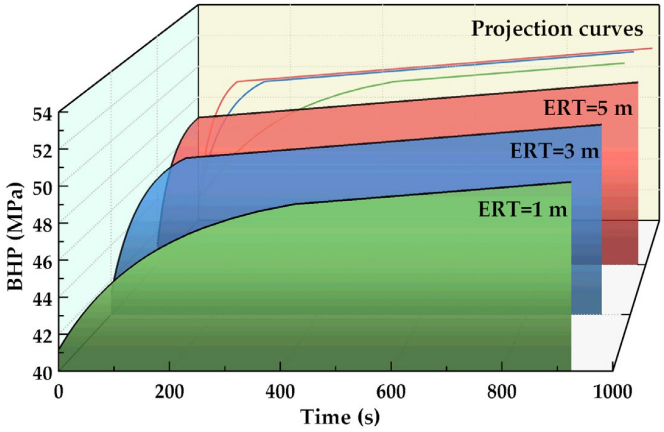


Figure 5. Variations in bottomhole pressure over time under different exposed reservoir thicknesses. The BHP represents bottomhole pressure, and the ERT represents exposed reservoir thickness.

3.3. Effect of Formation Permeability on Bottomhole Pressure

The simulation was conducted using an initial bottomhole pressure of 41.16 MPa, a fixed formation pressure of 50 MPa, and formation permeabilities of 10×10^{-3} μm^2, 20×10^{-3} μm^2, and 30×10^{-3} μm^2. The other parameters were the same as in Section 3.1. The simulated bottomhole pressure variations over time under different formation permeabilities are shown in Figure 6. It can be seen that in all cases, the bottomhole pressure increases over time, showing an initial rapid increase followed by a gradual slowdown in the rate of increase. The smaller the formation permeability, the longer it takes for the bottomhole pressure to reach the formation pressure. This is because the effect of the formation permeability on bottomhole pressure is primarily evident during the residual flow stage. Thus, during this stage, smaller formation permeabilities result in slower gas invasion rates, thereby extending the duration of the residual flow stage.

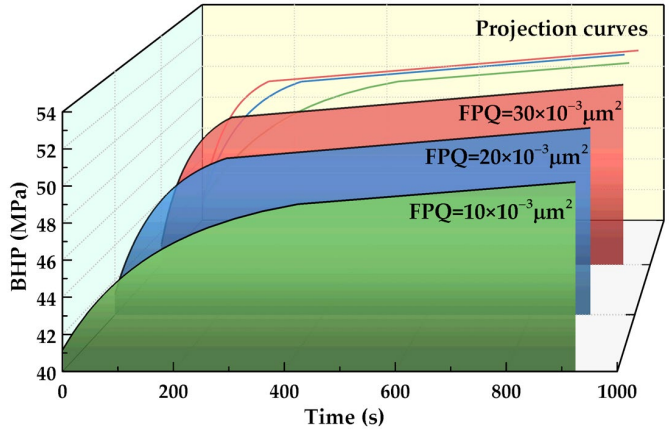


Figure 6. Variations in bottomhole pressure over time under different formation permeabilities. The BHP represents bottomhole pressure, and the FPQ represents formation permeability.

3.4. Effect of Filter Cake Permeability on Bottomhole Pressure

The simulation was conducted using an initial bottomhole pressure of 41.16 MPa, a fixed formation pressure of 50 MPa, and filter cake permeabilities of 1×10^{-4} μm^2, 1×10^{-6} μm^2, and 8×10^{-8} μm^2. The other parameters were the same as in Section 3.1.

The simulated bottomhole pressure variations over time under different filter cake permeabilities are shown in Figure 7. The results show that the smaller the filter cake permeability, the faster the bottomhole pressure rises. During the residual flow stage, where no drilling fluid loss occurs, the bottomhole pressure is unaffected by the filter cake permeability. The bottomhole pressure exhibits the same logarithmically increasing trend as it approaches the formation pressure. During the gas ascent stage, a smaller filter cake permeability results a slower rate of drilling fluid loss into the formation, which constrains the expansion due to the rising gas. As a result, the bottomhole pressure increases more rapidly.

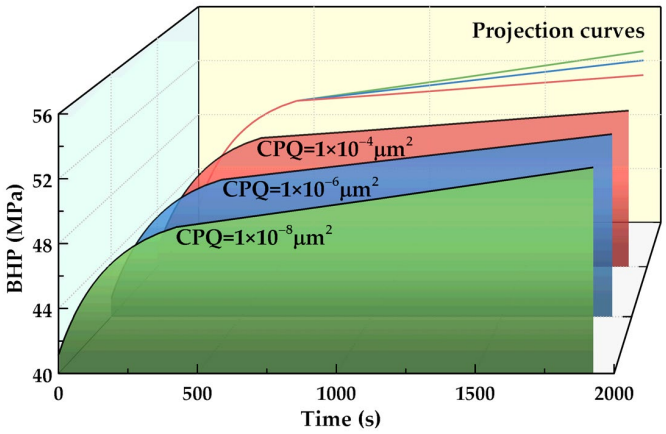


Figure 7. Variations in bottomhole pressure over time under different filter cake permeabilities. The BHP represents bottomhole pressure, and the CPQ represents filter cake permeability.

3.5. Effect of Drilling Fluid Density on Bottomhole Pressure

The simulation was conducted using a fixed formation pressure of 50 MPa and drilling fluid densities of 1000 kg/m^3, 1200 kg/m^3, and 1400 kg/m^3. The other parameters were the same as in Section 3.1. The simulated bottomhole pressure variations over time under different drilling fluid densities are shown in Figure 8. The results show that under varying drilling fluid densities, the bottomhole pressure initially rises rapidly and then increases slowly over time. The drilling fluid density primarily affects the initial bottomhole pressure; that is, a higher density results in a greater initial bottomhole pressure, leading to a smaller pressure differential at the bottom of the hole. Consequently, during the residual flow stage, as the drilling fluid density increases, the increment in bottomhole pressure is reduced, and the duration of this stage decreases.

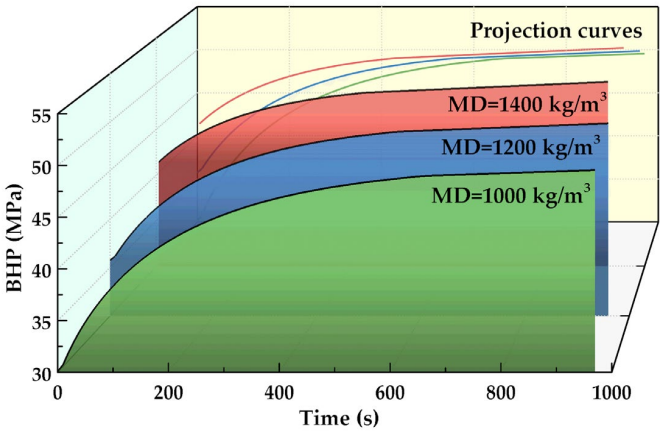


Figure 8. Variations in bottomhole pressure over time under different drilling fluid densities. The BHP represents bottomhole pressure, and the MD represents drilling fluid density.

3.6. Effect of Drilling Fluid Viscosity on Bottomhole Pressure

The simulation was conducted using an initial bottomhole pressure of 41.16 MPa, a fixed formation pressure of 50 MPa, and drilling fluid viscosities of 10 mPa·s, 20 mPa·s, and 30 mPa·s. The other parameters were the same as in Section 3.1. The simulated bottomhole pressure variations over time under different drilling fluid viscosities are shown in Figure 9. The results indicate that the higher the drilling fluid viscosity, the slower the bottomhole pressure rise. The drilling fluid viscosity primarily affects the velocity of gas ascent; that is, a higher viscosity results in a lower gas ascent. During the residual flow stage, the drilling fluid viscosity does not influence the bottomhole pressure. However, during the gas ascent stage, a higher drilling fluid viscosity results in a greater resistance of gas ascent, leading to a slower velocity of gas ascent. This reduces the rate of pressure increase due to gas expansion per unit time, consequently resulting in a slower rise in the bottomhole pressure.

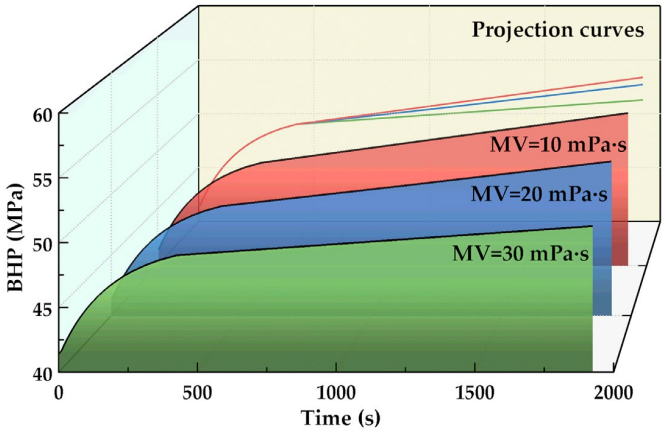


Figure 9. Variations in bottomhole pressure over time under different drilling fluid viscosities. The BHP represents bottomhole pressure, and the MV represents drilling fluid viscosity.

4. Conclusions

In this study, we addressed the shortcomings of existing models in predicting the bottomhole pressure under shut-in conditions during deepwater drilling. A bottomhole pressure prediction model that considers the storage effects of the wellbore was developed and validated through a case study. The findings of this study will provide theoretical guidance for well control operations during shut-ins in deepwater drilling. The main conclusions are summarized below.

1. The developed model incorporates factors such as the wellbore elasticity, fluid compressibility, and drilling fluid filtration loss, enabling a more accurate description of wellbore pressure variations during shut-in operations in deepwater drilling. The new model shows good agreement with the experimental values, with the average absolute and relative errors of 2.095×10^{-2} MPa and 3.71%, respectively.
2. The variation trends of the bottomhole pressure during shut-ins in deepwater drilling were elucidated. The bottomhole pressure initially increases logarithmically and then transitions to a linear increase over time. In the early stages of a shut-in, the residual flow is the primary controlling factor, whereas the gas ascent becomes the primary controlling factor after the bottomhole pressure exceeds the formation pressure.
3. The effects of formation pressure, exposed reservoir thickness, formation permeability, filter cake permeability, drilling fluid density, and viscosity on the bottomhole pressure were evaluated using the new model. The larger initial pressure differential, exposed thickness, and formation permeability all contributed to more rapid increases in bottomhole pressure during the residual flow stage. The smaller filter cake permeability and drilling fluid viscosity caused a quicker rise in bottomhole pressure during

the gas ascent stage. The drilling fluid density affected the initial pressure and the duration of the residual flow stage.

Author Contributions: Y.G. (Yanli Guo), conceptualization, methodology, and writing—original draft preparation; Y.G. (Yonghai Gao), methodology and investigation; Q.G., methodology and project administration; L.H., writing—review and editing; Y.J., investigation and formal analysis; B.S., conceptualization and resources. All authors have read and agreed to the published version of the manuscript.

Funding: This research was funded by the Shandong Provincial Natural Science Foundation, China, grant number ZR2020QE114 and ZR2023QE323, and the National Natural Science Foundation of China, grant number 52371325.

Institutional Review Board Statement: Not applicable.

Informed Consent Statement: Not applicable.

Data Availability Statement: Data are contained within the article.

Conflicts of Interest: The authors declare no conflicts of interest.

References

1. Yang, H.; Li, J.; Zhang, G.; Zhang, H.; Guo, B.; Chen, W. Wellbore multiphase flow behaviors during gas invasion in deepwater downhole dual–gradient drilling based on oil–based drilling fluid. *Energy Rep.* **2022**, *8*, 2843–2858. [CrossRef]
2. Chen, T.; Guan, Z. *Drilling Engineering Theory and Technology*, 1st ed.; China University of Petroleum Press: Dongying, China, 2006; pp. 1–5.
3. Jia, X.; Li, Y.; Zhao, T. State–of–the–art and overall configuration of drilling system equipment for ocean drilling vessels. *Ship Boat* **2023**, *34*, 67–76.
4. Johnson, A.S.; Smith, G.D. The technology of drilling in 7500 ft of water. In Proceedings of the SPE California Regional Meeting, Long Beach, CA, USA, 11–13 April 1984.
5. Jahanpeyma, Y.; Jamshidi, S. Two–phase simulation of well control methods for gas kicks in case of water and oil–based muds. *J. Pet. Sci. Technol.* **2018**, *8*, 34–48.
6. Lei, Y.; Sun, J.; Wang, G. Simulation of shallow gas invasion process during deepwater drilling and its control measures. *J. Ocean Univ. China* **2022**, *21*, 707–718. [CrossRef]
7. Li, Q.; Li, Q.; Han, Y. A numerical investigation on kick control with the displacement kill method during a well test in a deep–water gas reservoir: A case study. *Processes* **2024**, *12*, 2090. [CrossRef]
8. Li, Q.; Zhou, S.; Zhao, J.; Song, Y.; Zhu, J. Research status and prospects of natural gas hydrate exploitation technology. *Strateg. Study Chin. Acad. Eng.* **2022**, *24*, 214–224. [CrossRef]
9. Fu, W.; Zhao, Z.; Yu, J.; We, W.; Wang, Z.; Huang, B. Prediction model of hydrate formation in bubbly flow and experimental study. *Chem. Ind. Eng. Prog.* **2022**, *41*, 5746–5754.
10. Li, J.; Yang, H.; Zhang, H.; Wang, J.; Gao, R.; Zhang, R. Progress of basic research on wellbore pressure control in deepwater oil and gas drilling and production. *Bull. Natl. Nat. Sci. Found. China* **2021**, *35*, 973–983.
11. Li, Z.; Yin, Z.; Tian, D. Research progress on well control risk management technology for deep sea and ultra–deep water drilling. *Drill. Prod. Technol.* **2024**, *47*, 8–17.
12. Sun, B.; Wang, Z.; Gong, P.; Song, R. Application of a seven–component multiphase flow model to deepwater well control. *Acta Pet. Sin.* **2011**, *32*, 1042–1049.
13. Wang, Z. Study on Annular Multiphase Flow Pattern Transition Mechanism Considering Gas Hydrate Phase Transition. Doctoral Dissertation, China University of Petroleum (East China), Qingdao, China, April 2009.
14. Ren, M.; Li, X.; Liu, S.; Wang, Y. Characteristics of wellbore pressure change during shut–in after blowout. *J. China Univ. Pet.* **2015**, *39*, 113–119.
15. Wan, L.; Li, G.; Chi, H.; Song, X.; Wang, H. Research on the principles of wellbore multiphase flow during sour gas influx. *Fluid Mach.* **2012**, *40*, 19–23.
16. He, M. Study on Real Time Interpretation Theory and Control Method of Managed Pressure Drilling Overflow. Doctoral Dissertation, China University of Petroleum (Beijing), Beijing, China, April 2016.
17. Halkyard, J.; Anderson, M.R.; Maurer, W.C. Hollow glass microspheres: An option for dual gradient drilling and deep ocean mining lift. In Proceedings of the Offshore Technology Conference Asia, Kuala Lumpur, Malaysia, 25–28 March 2014.

18. Marbun, B.T.; Kurnia, H.A. The effect of high pressure and temperature variation to the hydraulic of dual gradient drilling operation. In Proceedings of the IADC/SPE Asia Pacific Drilling Technology Conference and Exhibition, Tianjin, China, 9–11 July 2012.
19. Li, J. Study on Wellbore Flow Mechanics and Pressure Control in Deep–Water Controlled Mud Level Dual Gradient Drilling. Doctoral Dissertation, China University of Petroleum (Beijing), Beijing, China, April 2016.
20. Xu, C. Research on the Numerical Algorithm for Transient Multiphase Flow and Response Characteristics of Flow Parameters in Wellbore. Doctoral Dissertation, Southwest Petroleum University, Chengdu, China, June 2015.
21. Rashid, F.L.; Hussein, H.Q.; Bded, A.S. Numerical simulation of fluid flow and heat transfer in wellbore. *J. Adv. Res. Fluid Mech. Therm. Sci.* **2019**, *60*, 60–70.
22. Leblanc, J.L.; Lewis, R.L. A mathematical model of a gas kick. *J. Pet. Technol.* **1968**, *20*, 888–898. [CrossRef]
23. Yan, J. *Drilling Fluid Technology*, 1st ed.; China University of Petroleum Press: Dongying, China, 2006.
24. Dranchuk, P.M.; Purvis, R.A.; Robinson, D.B. Computer calculations of natural gas compressibility factors using the Standing and Katz correlation. *Inst. Pet. Tech. Ser.* **1974**, *36*, 76–80.
25. Lee, A.; Gonzalez, M.; Eakin, B. The viscosity of natural gases. *J. Pet. Technol.* **1966**, *18*, 997–1000. [CrossRef]
26. Guo, Y.; Liu, W.; Song, C.; Gong, Q.; Teng, Y. Seepage–diffusion mechanism of gas kick considering the filtration loss of oil–based muds during deepwater drilling. *J. Mar. Sci. Eng.* **2024**, *12*, 2035. [CrossRef]
27. Anagbo, P.E.; Brimacombe, J.K.; Wraith, A.E. Formation of ellipsoidal bubbles at a free–standing nozzle. *Chem. Eng. Sci.* **1991**, *46*, 781–788. [CrossRef]
28. Li, X.; Zhuang, X.; Sui, X.; Gang, T. Study on two–phase gas–liquid flow during gas kick. *J. Eng. Thermophys.* **2004**, *25*, 73–76.
29. Zhang, L.; Liu, Z.; Sun, B.; Yu, X.; Liu, K. Experimental study on the changing characteristics of bottom–hole pressure during the overflow shut–in period and its influencing factor analysis. In Proceedings of the 2019 International Petroleum and Petrochemical Technology Conference, Beijing, China, 27–29 March 2019.

Disclaimer/Publisher's Note: The statements, opinions and data contained in all publications are solely those of the individual author(s) and contributor(s) and not of MDPI and/or the editor(s). MDPI and/or the editor(s) disclaim responsibility for any injury to people or property resulting from any ideas, methods, instructions or products referred to in the content.